HHS Public Access

Author manuscript

J Cardiovasc Comput Tomogr. Author manuscript; available in PMC 2024 May 01.

Published in final edited form as:

J Cardiovasc Comput Tomogr. 2023 ; 17(3): 201–210. doi:10.1016/j.jcct.2023.03.009.

Endothelial Shear Stress Computed from Coronary Computed Tomography Angiography: A Direct Comparison to Intravascular Ultrasound

Diaa Hakim[a], **Ahmet U Coskun**[b], **Charles Maynard**[c], **Zhongyue Pu**[d], **Deborah Rupert**[e], **Nicholas Cefalo**[a], **Michelle Cormier**[a], **Mona Ahmed**[a,j], **James Earls**[f], **Rob Jennings**[f], **Kevin Croce**[a], **Saima Mushtaq**[h], **Daniele Andreini**[h], **Edoardo Conte**[h], **David Molony**[i], **Habibi Samady**[i], **James K Min**[f], **Peter H Stone**[a]

[a]-Cardiovascular Division, Brigham & Women's Hospital/Harvard Medical School, Boston, MA, USA

[b]-Department of Mechanical and Industrial Engineering, Northeastern University, Boston, MA, USA

[c]-Department of Health Systems and Population Health, University of Washington, Seattle, WA, USA

[d]-Department of Medical Science, Nagoya University Graduate School of Medicine, Nagoya, Japan

[e]-Medical Scientist Training Program, Stonybrook University, New York, NY, USA

[f]-Cleerly Laboratory, Cleerly Inc, Denver, Co, USA

[h]-Department of University Cardiology and Cardiac Imaging, IRCCS Ospedale Galeazzi Sant'Abrogio, and Department of Biomedical and Clinical Sciences, University of Milan, Milan, Italy

[i]-Northeast Georgia Health System, Gainesville, GA, USA

[j]-Department of Molecular Medicine and Surgery, Karolinska Institute, Karolinska University Hospital Solna, Stockholm, Sweden

Address for Correspondence: Peter H. Stone, MD, Division of Cardiovascular Medicine, Brigham & Women's Hospital, 75 Francis Street, Boston, Massachusetts, U.S.A 02115, pstone@bwh.harvard.edu, Fax: 307-1955.

Declaration of interests

The authors declare that they have no known competing financial interests or personal relationships that could have appeared to influence the work reported in this paper.

Conflict of Interest

- Peter H. Stone has the following disclosures: Research support from NIH, and Generous support from the Schaubert Family
- James K. Min has the following disclosures: GE Healthcare, Arineta, Ownership Interest, Research Grant from GE Healthcare.
- James Earls and Rob Jennings are working for Cleerly
- Kevin Croce has the following disclosures: Honoraria from; CSI, Abbott, Philips, Abiomed, Cordis
- No disclosure for the other co-authors related to this abstract

Abstract

Introduction: Intravascular ultrasound (IVUS) studies have shown that biomechanical variables, particularly endothelial shear stress (ESS), add synergistic prognostic insight when combined with anatomic high-risk plaque features. Non-invasive risk assessment of coronary plaques with coronary computed tomography angiography (CCTA) would be helpful to enable broad population risk-screening

Aim: To compare the accuracy of ESS computation of local ESS metrics by CCTA vs IVUS imaging.

Methods: We analyzed 59 patients from a registry of patients who underwent both IVUS and CCTA for suspected CAD. CCTA images were acquired using either a 64- or 256-slice machine. Lumen, vessel, and plaque areas were segmented from both IVUS and CCTA (59 arteries, 686 3-mm segments). Images were co-registered and used to generate a 3-D arterial reconstruction, and local ESS distribution was assessed by computational fluid dynamics (CFD) and reported in consecutive 3-mm segments.

Results: Anatomical plaque characteristics (vessel, lumen, plaque area and minimal luminal area [MLA] per artery) were correlated when measured with IVUS and CCTA: 12.7 ± 4.3 vs 10.7 ± 4.5 mm^2, r=0.63; 6.8 ± 2.7 vs 5.6 ± 2.7 mm^2, r=0.43; 5.9 ± 2.9 vs 5.1 ± 3.2 mm^2, r=0.52; 4.5 ± 1.3 vs 4.1 ± 1.5 mm^2, r= 0.67 respectively. ESS metrics of local minimal, maximal, and average ESS were also moderately correlated when measured with IVUS and CCTA (2.0 ± 1.4 vs 2.5 ± 2.6 Pa, r=0.28; 3.3 ± 1.6 vs 4.2 ± 3.6 Pa, r=0.42; 2.6 ± 1.5 vs 3.3 ± Pa, r=0.35, respectively). CCTA-based computation accurately identified the spatial localization of local ESS heterogeneity compared to IVUS, with Bland-Altman analyses indicating that the absolute ESS differences between the two CCTA methods were pathobiologically minor.

Conclusion: Local ESS evaluation by CCTA is possible and similar to IVUS; and is useful for identifying local flow patterns that are relevant to plaque development, progression, and destabilization.

Keywords

Coronary Computed Tomography Angiography; CCTA, Intravascular Ultrasound; IVUS, Endothelial Shear Stress; ESS

1. INTRODUCTION

Risk-stratification of individual coronary plaques is an important goal to identify high-risk plaques that are likely to progress or destabilize, information that may enable preemptive interventions to prevent major adverse cardiac events (MACE). Early prognostic studies utilized invasive intravascular imaging with intravascular ultrasound (IVUS) and optical coherence tomography (OCT) and focused mainly on anatomic plaque characteristics such as minimal lumen area, plaque burden, necrotic core, fibrous cap thickness,[1–3] as well as biochemical characteristics such as lipid pool.[4–6] Natural history outcome studies demonstrated, however, that while anatomic plaque characteristics provide the essential substrate to understand plaque behavior and disease prognosis, the majority of these ostensibly high-risk plaques remain quiescent and do not destabilize to cause

clinical events.[7–9] More recent prognostic plaque investigations have broadened the risk-stratification focus to include local biophysical features, such as endothelial shear stress (ESS)—the frictional force of blood acting on endothelial cells which drives plaque development and progression[10,11]—which acts synergistically with anatomic high-risk features to trigger plaque destabilization and MACE.[2,12,13]

Invasive intravascular imaging is the current gold standard to assess plaque characteristics and plaque risk, but its widespread application is limited by its invasive nature, high-cost and requirement for detailed offline analyses that are time-consuming and require substantial technical and computational resources. In contrast, non-invasive plaque risk-assessment with coronary computed tomography angiography (CCTA) would be invaluable for broad population-based risk screening, as well as serial assessments for patients with known coronary artery disease (CAD), since it is non-invasive, inexpensive, enables whole imaging of the entire coronary artery tree, and ESS computation could potentially be completed and reported at the point-of-care. Previous CCTA studies have clearly shown that assessment of plaque burden and calcium score provides important diagnostic and prognostic information not only about stenotic atherosclerotic plaques but also early atherosclerotic lesions.[14–17] Specific high-risk plaque features, such as low attenuation, positive remodeling, napkin ring sign, and spotty calcification serve as independent predictors of future acute coronary syndromes.[15,18]

CCTA image resolution, however, is less precise than invasive IVUS or OCT imaging, and so its predictive accuracy for optimal risk-stratification including characterization of the local biomechanical ESS surrounding individual plaques remains unclear. The aim of the present study, therefore, was to compare the accuracy of ESS computation of local ESS metrics by non-invasive CCTA vs invasive IVUS imaging. This foundational study was designed to enable larger non-invasive studies to confirm the nature of the biomechanical characteristics of coronary atherosclerotic plaques and the prognostic value of non-invasive imaging compared to invasive imaging.

2. METHODS

2.1. Patient population:

We analyzed 118 patients identified from a recently published Italian registry who underwent CCTA imaging, and invasive coronary angiography and IVUS, within 90 days of one another, for suspected, but without previously known, CAD, that compared calculation of plaque volume measurements by the non-invasive vs invasive modality.[19] Patients were divided into two groups based on the CCTA imaging method employed: 59 patients who underwent 64-slice CCTA, and 59 patients who underwent 256-slice CCTA.

2.2. CCTA Image Acquisition:

In patients imaged with a 64-slice scanner, Discovery CT 750 HD scanner (GE Healthcare, Milwaukee, WI, USA) was used with the following parameters: slice configuration 64X 0.625 mm and gantry rotation time 350 ms. A first-generation iterative reconstruction algorithm (ASIR, GE Healthcare, Milwaukee, WI, USA) and a BMI-adapted scanning

protocol were used. A bolus of 70 mL (for BMI 25 kg/m2) of high concentration contrast (Iomeron 400 mg/mL, Bracco Imaging, Milan, Italy) was administered, and the scan was initiated according to the bolus-tracking technique.

In the patients imaged with a 256-slice scanner, Revolution CT (GE Healthcare, Milwaukee, WI, USA) was used to perform CCTA with the following parameters: slice configuration 256 X 0.625 mm, gantry rotation time 280 ms and prospective ECG triggering. A new generation of iterative reconstruction (ASIR-V, GE Healthcare, Milwaukee, WI, USA) was used. Tube current and tube voltage were adapted to BMI.13 Patients received a 50-mL (for BMI 25 kg/m2) bolus of contrast medium (Iomeron 400 mg/mL, Bracco, Milan, Italy). Imaging was performed using the bolus-tracking technique. Sublingual nitrates and intravenous beta-blockers (metoprolol with dose up to 20 mg, according to heart rate) were administered before the CCTA scan in both groups.

2.3. IVUS Image Acquisition:

IVUS images were obtained within 90 days from the time of the CCTA acquisition. All procedures were performed for clinical indications. Imaging was performed after intracoronary administration of 200 μg nitroglycerin using a 40 MHz OPTICROSS IVUS catheter (Boston Scientific Corporation, Fremont, CA) and automatic pullback at a speed of 0.5mm/sec. For each cross-sectional image the external elastic membrane (EEM) and the luminal interface were detected and traced.

2.4. Identification of Imaging Datasets Adequate for both CCTA and IVUS Image Analysis:

Original IVUS, coronary angiography, and CCTA images were transferred to the Vascular Profiling Laboratory at Brigham & Women's Hospital (Boston, MA), where blinded segmentation of IVUS images were performed. CCTA segmentation and image analysis was similarly performed in a blinded fashion at the Cleerly laboratories (Cleerly Inc, Denver, CO).

CFD analyses were performed on both the noninvasive and invasive segmented imaging datasets using the centerline derived from the CCTA images for the IVUS 3-D image reconstruction, and we compared the respective results of the ESS computations using CCTA and IVUS imaging.

2.5. Artificial Intelligence (AI)-Based CCTA Segmentation and Centerline Generation:

An AI-enabled approach to CCTA segmentation and analysis in this study was performed using an FDA-approved software (Cleerly Laboratory, Cleerly, Denver, CO) that performs automated analysis of CCTA using a series of validated convolutional neural network models (including VGG19 network, 3D U-Net, and VGG Network Variant) for image quality assessment, coronary segmentation and labeling, lumen boundary evaluation, vessel contour determination and plaque characterization. First, the AI-aided approach produces a centerline along each coronary artery, and then for lumen and vessel wall contouring. This is applied to each phase of the examination and the optimal series are identified for further analysis. These top phases are evaluated interactively on a per vessel basis, e.g., the right coronary artery (RCA) will be reconstructed from the phase which yields the

highest RCA image quality, while the posterior descending artery (PDA) may come from the second phase if the PDA has a higher image quality on that phase. Once coronary artery segmentation is performed, automated labeling is done to classify arteries by their location as well the proximal, mid, and distal portions within a single vessel. After the AI algorithm has finished all operations, a quality control cardiac CT-trained technologist reviews the results of the AI analysis and makes manual adjustment if necessary (in less than 10% of cases). A dataset containing the coronary artery centerline as well as the location of the lumen and vessel wall were exported for co-registration purposes with the IVUS exams.

2.6. IVUS data Analysis:

IVUS images were gated at the same cardiac phase, so that diameter variations due to cardiac contraction were removed. IVUS segmentations of the lumen and EEM were manually conducted using an in-house segmentation software at the Vascular Profiling Laboratory at Brigham & Women's Hospital. We extracted the segmented lumens at each cross-section as point clouds at each gated frame for IVUS. We adapted this methodology which enabled us to fuse the contours segmented based on invasive imaging with the 3D centerline extracted from CCTA. Qualitative and quantitative analyses were performed according to the criteria of the American College of Cardiology Clinical Expert Consensus Document on Standards for Acquisition, Measurements, and Reporting of IVUS Studies.[20]

2.7. Co-Registration of IVUS and CCTA Segmentation:

We compared CCTA vs IVUS images side by side for the co-registration to define the culprit vessel then we defined the plaque length in both imaging modalities using a fiduciary point such as minimal luminal area, calcified plaques and side branches to match the region of interest in both imaging modalities. We used a large side branch as our proximal landmark, such as the left main bifurcation site if the culprit vessel was the LAD or LCX in both IVUS and CCTA and we used the most distal branch as our distal landmark in both imaging modalities. Further, we used coronary angiograms acquired at the time of IVUS to keep track of the location of branches relative to each other.(Figure 1S)

2.8. Three-D Reconstruction of Coronary Arteries and Computational Fluid Dynamics (CFD) Calculations:

Images from CCTA and IVUS were fused to create a 3D coronary reconstruction based on the 2D-lumen segmentations from IVUS. We fused the 2-D point clouds of lumen/EEM borders extracted from IVUS segmentation with the 3-D-centerline extracted from the CCTA. As a first step in the fusion process, a segment of interest that was common both in IVUS and CTA acquisition was identified using branch locations. Distal and proximal IVUS frames and corresponding locations on CTA were marked. A smoothing cubic-spline curve was fitted for the center line of CCTA geometry. Locations of the IVUS frames on the smooth centerline were determined by interpolating distance measured on the centerline of IVUS frames to match the distance measured on the smooth CCTA geometry centerline for the segment of interest. Then, the 2-D point cloud data representing borders on IVUS frames were isotopically transformed such that the lumen centroid coincided with the CT-based centerline points and the normal to the cross sections were aligned with the local curvature tangent of the centerline. In addition, to ensure correct orientation as well as the rotation of

each cross-section, we used the landmarks in the co-registration process (as described above) and compared each consecutive cross-section's normal to ensure their dot-products were positive. The boundary points of each frame were connected by spline curves to rebuild the luminal geometry in 3-D space. A structured grid that used a body-fitted coordinate system was employed to represent the lumen volume. The lumen was divided into computational control volumes comprising 0.3-mm-thick slices along the segment, 40 equal intervals around the circumference (lumen interface), and 24 progressively narrowing intervals in the radial direction from the center of the reconstructed lumen to the lumen surface. A volume average velocity of 0.172 m/s was used as the volumetric flow rate for each vessel based on the average values obtained from a different data set with large number of arteries of which coronary blood flow rates were measured by dividing the true 3D volume of the segment, calculated from the lumen borders as described above, by the time required for the volume of blood contained within the same section to be displaced by radio-opaque material during a contrast injection utilizing timing of cine frames. The region of interest for flow calculation was chosen as a segment free of significant side branches that may significantly alter the flow through the segment under investigation.

The detailed intravascular flow characteristics were obtained by solving the transport equations governing the conservation of mass and momentum utilizing a simple Foam simulation program within Open FOAM CFD platform. We assumed that the arterial wall was stiff, and that blood was incompressible, homogeneous steady flow, and Newtonian. A parabolic fully developed velocity profile was assumed at the inlet boundary. In the simulations, pressure solution was achieved using GAMG Multi-Grid Solver with GaussSeidel smoother, tolerance was set to 10^{-6} and minimum number of iterations was set to 2. Velocity solution was achieved using PBiCG Linear Solver with DILU preconditioner, tolerance was set to 10^{-8} and minimum number of iterations was set to 3. Momentum predictor is enabled. Convergence Tolerance was set to 10^{-10} for both pressure and velocity.

2.9. Statistical Analysis

Categorical variables were presented as numbers and proportions, and continuous variables were reported as means and standard deviations. We used the Chi-square statistic to compare categorical variables. For continuous variables, we used the Pearson r correlation coefficient to examine the association between IVUS and CCTA for the following variables: lumen area, vessel area, plaque area, MLA, average ESS, plaque 90° arc minimum ESS, plaque 90° arc maximum ESS and plaque 90° arc average ESS. For each 3-mm segment, plaque 90° arc minimum ESS was defined as the minimum ESS value over a rotating 90° arc around the vessel circumference, plaque 90° arc maximum ESS was defined as the maximum ESS value over a rotating 90° arc around the vessel circumference, and plaque 90° arc average ESS was defined as the average ESS value over a rotating 90° arc around the vessel circumference.[22] We further examined associations for these variables for combined 256 and 64-slice CCTA, 256-slice only, and 64-slice only and assessed whether the correlation coefficients for IVUS and CCTA were statistically different with the Fisher r to z transformation. Instead of testing that the correlation coefficient is different from 0, we used a p-value which indicates whether the correlation coefficient is different from a modest correlation of 0.25. For plaque 90° arc minimum ESS, plaque 90° arc maximum ESS and

plaque 90° arc average ESS, we calculated the mean difference between IVUS and CCTA for combined 256-and 64-slice CCTA, 256-slice only, and 64-slice only. Linear regression was used to determine whether these differences were statistically different. Standard errors of the regression coefficients were adjusted for correlated error using the Huber-White Sandwich Estimator. Finally, Bland-Altman plots were used to further explore the agreement between IVUS and CCTA for each of the three variables of interest. We also used the unweighted Kappa statistic to examine the level of agreement between CCTA and IVUS for categories of ESS. Comparisons were made for all CCTA, 256 slice, and 64 slice.

3. RESULTS

3.1. Patient Cohort:

Of the 118 patient datasets only 59 (50%) were technically adequate for CFD computations using both CCTA and IVUS images (30 patients using 64-slice CCTA and 29 patients using 256-slice CCTA). Figure 1 shows the study flow chart and reasons for excluding patients. The IVUS imaging methods were similar regardless of which CCTA scanner modality was employed. The patients' demographic and clinical data are presented in Table 1.

3.2. Comparison of CCTA (Combined 64-slice and 256-slice) vs. IVUS Anatomic Plaque Characteristics and ESS Metrics:

Vessel area, lumen and plaque areas and MLA per artery measured with IVUS were strongly correlated to those measured with CCTA (12.7 ± 4.3 vs 10.7 ± 4.5 mm^2, r=0.63; 6.8 ± 2.7 vs 5.6 ± 2.7 mm^2, r = 0.43: 5.9 ± 2.9 vs. 5.1 ± 3. mm^2, r = 0.52; and 4.5 ± 1.3 vs 4.1 ± 1.5 mm^2, r = 0.67, respectively; each $p<0.0001$) (Table 2).

ESS metrics of average ESS, minimal ESS, maximal ESS were also significantly correlated when measured with CCTA and IVUS (2.6 ± 1.5 vs 3.3 ± 3.0 Pa, r=0.35; 2.0 ± 1.4 vs 2.5 ± 2.6 Pa, r=0.28; and 3.3 ± 1.6 vs 4.2 ± 3.6 Pa, r=0.42, respectively, each $p<0.0001$)

Figure 2 illustrates images of a representative patient's 3-D reconstruction and color-coded topographical map displaying the values of lumen radius, vessel radius, plaque thickness and ESS metrics computed from both CCTA and IVUS imaging. There is excellent correlation in the metrics between the two modalities, including the detailed heterogeneity of plaque contours and local ESS values.

3.3. Comparison of CCTA (separately 64-slice and 256-slice) vs IVUS Anatomic Plaque Characteristics and ESS Metrics:

To determine the effect of differences in CT technology, we also performed a subgroup analysis of ESS metrics by CCTA with 64-slice compared to 256-slice CT. Within each type of CCTA method (64-slice or 256-slice) the plaque anatomic and ESS metrics were highly correlated with the metrics derived by IVUS imaging (Table 3). The correlation coefficients were numerically higher for the 256-slice imaging modality and IVUS metrics compared to the 64-slice imaging modality and IVUS ESS metrics, but none of these differences were statistically significant (Table 3).

3.4. Categorical Local ESS measurements:

We examined the agreement between CCTA and IVUS for categories of ESS defined as: 1) low ESS [<1.0 Pa], 2) physiologic ESS [1.0–2.5Pa], 3) high ESS [2.5–5.0 Pa], 4) higher ESS [5.1–7.0 Pa] and 5) very high ESS [>7.0 Pa] .There was modest agreement between the 2 modalities for all CCTA, 256 slice, and 64 slice, as indicated by Kappa statistics from 0.20 to 0.26 (Table 4). In general, there were higher levels of ESS in CCTA as compared to IVUS; this was particularly true for 64 slice CCTA where 14.2% were in the very high category as opposed to only 2.8% in IVUS. Table 5 illustrates the comparison of categories of ESS by per-segment analysis for all CCTA formats vs IVUS. Per-segment categorical comparison of the ESS (Low: <1 Pa; Physiological: 1–2.5 Pa; High: 2.5–5 Pa; Higher: >5–7 Pa; and Very High: >7 Pa) between CCTA and IVUS showed exact agreement 52.9% of the time for measurement of average ESS, 46.9% of the time for the measurement of min ESS, and 48.5 % of the time for measurements of the max ESS. Similarly, the agreement within one category was 79.8% of time for the measurement of average ESS, 70.8% of the time for the measurement of Min ESS, and 88.5% of the time for measurement of Max ESS (Agreement for average ESS, kappa=0.25, $p<0.0001$; agreement for min ESS, kappa=0.20, $p<0.0001$; and agreement for max ESS, kappa=0.22, $p<0.0001$).

3.5. Bland-Altman Plots of ESS Metrics by CCTA (combined or separate 64-slice and 256-slice) Compared to ESS Metrics by IVUS:

Figures 3–5 illustrate the Bland-Altman plots comparing the CCTA-derived metrics (combined 64-slice and 256-slice) and the IVUS-derived metrics for Minimal ESS, Maximal ESS, and Average ESS, respectively. The Bland-Altman plots for the separate 64-slice and the 256-slice CCTA-derived metrics and the IVUS-derived metrics are presented in Figures 2S-7S in the Supplementary Material. The mean differences in the ESS metrics as measured by IVUS versus the different CCTA imaging methods are presented in Table 5. Although these differences are statistically significant, the absolute value of the differences are not pathobiologically or clinically meaningful. The Bland-Altman plots demonstrated a funnel shape indicating higher ESS in the CCTA modality.

4. DISCUSSION

In this present study, we sought to compare the accuracy of non-invasive CCTA imaging-based ESS computation to invasive IVUS-based ESS computation—the current gold standard—to evaluate both the local heterogeneous and the average ESS patterns. We further performed a subgroup analysis to compare the accuracy of the 256- vs the 64-slice CCTA imaging-based CFD vs IVUS-based CFD. Our main findings are: (1) Categorizing the heterogeneous local ESS environment within individual arteries, from low ESS through very high ESS, the CCTA-based methods identify the spatial localization of heterogeneity accurately compared to the localization by IVUS-based imaging, with Bland-Altman analyses indicating that the absolute ESS difference in Pa between the two CCTA methods are pathobiologically minor; and (2) Compared to IVUS-based values, 256-slice CCTA and 64-slice CCTA are similar to measure lumen and vessel areas and for the computation of detailed local ESS values (Average ESS, Minimum ESS, Maximum ESS). In summary we observed moderate correlations and statistically significant differences in mean bias between

CCTA and IVUS. Further, there was a trend toward higher ESS in CCTA, especially in the 64-slice group. This finding was demonstrated in the funnel shaped Bland-Altman plots. When ESS was defined as a categorical variable, there was modest agreement for all CCTA, 256 slice, and 64 slice.

4.1. Invasive Risk-Assessment of Individual Coronary Plaques

Our present study findings advance the previously published scientific literature that has relied primarily upon invasive methods for determining ESS. Most previous studies investigating where coronary plaques develop, progress, and ultimately destabilize have utilized invasive imaging of IVUS or OCT.[1,9,21] A large plaque burden is typically the anatomic substrate for subsequent plaque progression and destabilization, and these plaques need not encroach substantially into the lumen and obstruct blood flow. Low ESS is typically responsible for the development and progression of plaque, since it triggers a local potent pro-inflammatory, pro-atherogenic, and pro-thrombotic phenotype.[1,10,22] Once established, the plaque may become destabilized and lead to MACE if it resides in either a local pathobiologically low or high ESS environment.[2,12]

The role of invasive risk-assessment, however, is fundamentally limited since only a small minority of patients with CAD undergo invasive evaluation, and the majority of patients truly at high-risk remain undetected. If it were possible to accurately predict those patients at risk for plaque destabilization and MACE in a non-invasive manner, such as with CCTA, the paradigm for meaningful risk assessment for patients with, or at risk for, CAD would considerably change.

4.2. Value of Non-invasive Risk Assessment of Individual Plaques

Due to limited resolution and associated artifacts, CCTA-derived computation to evaluate ESS metrics has been relatively uncommon compared with intravascular-based computation. In concordance with previous intravascular-based ESS studies, plaque prevalence was highest in areas of low and high ESS coronary segments computed using CCTA.[23] Further exploratory work has been conducted for ESS calculation using 320-slice CCTA. The calculation of ESS was conducted in the past using custom MUPHY Lattice Boltzmann software and was used in prediction of coronary artery plaque progression and potential rupture, but was severely limited by poor CCTA resolution.[24]

In another study, Park et al, investigated the distribution of hyperemic ESS with respect to CCTA-defined adverse plaque characteristics (APC) and showed that plaques exposed to the highest tertile of ESS formed a significant proportion of high-risk plaques, and ESS was found to have a superior value over luminal narrowing for the discrimination of APC.[25] Similarly, the EMERALD study investigated the utility of CCTA and CFD-derived hemodynamic parameters for the identification of high-risk plaques responsible for an acute coronary syndrome.[15] Seventy-two patients (66 culprit and 150 non-culprit lesions) with ACS underwent assessment of ESS and APCs. The study focused on evaluating non-invasive fractional flow reserve measured by computed tomography (FFRCT), ΔFFRCT, ESS, and axial plaque stress as derived from the CCTA. The results showed that this non-invasive assessment of local hemodynamic characteristics enhanced the identification of

high-risk plaques that subsequently caused ACS as compared to “anatomic” adverse plaque characteristics alone. Culprit lesions were found to have significantly higher mean ESS, ΔFFRCT, and axial plaque stress and a lower FFRCT, than non-culprit lesions.

It is notable to underscore, however, that previous non-invasive CCTA prognostic studies have been limited by using the single metric of “average ESS” alone, which masks the important details of the pathobiologic low ESS in particular, since the low Pa value is subsumed by the adjacent high ESS values in the process of averaging. This loss of appreciation of the role of local low ESS may be particularly germane in areas of high or very high ESS, since these areas are typically located immediately adjacent to areas of low ESS, and this high “ESS gradient” has been found to be an important pathophysiologic trigger for plaque rupture and erosion.[13,26] In the present study using current generation CCTAs we show for the first time the utility of non-invasive CCTA imaging-based computation to assess the detailed regional heterogeneity of ESS metrics that include average ESS, minimum ESS, and maximum ESS. We also demonstrate the similarity of CCTA-based ESS computations compared with IVUS-based computation to evaluate both continuous and categorical ESS variables.

4.3. Intravascular vs Non-invasive Imaging for ESS Evaluation

For the CCTA-based ESS computation to emerge as an alternative prognostication method to the invasive intravascular imaging-based computation, the relationships between the two imaging modalities need to be better understood. Bulant et al.[27] performed a comparison of hemodynamic parameters between fused angiography-IVUS reconstructions and CCTA reconstructions and observed that hyperemic ESS was higher in CCTA-reconstructed coronary arteries due to the apparent presence of a smaller lumen by CCTA measurement. This was attributed to lower CCTA resolution, presence of calcifications, and reduced pixel intensity in distal vascular regions. In another study, CCTA-based ESS calculations were compared to the ESS calculations using the gold-standard of fusion of invasive imaging and CCTA. In 14 patients paired patient-specific CFD models based on invasive and non-invasive imaging of the LAD coronary arteries were created. Ten patients were used to optimize the methodology, and four patients to test this methodology. Time-averaged ESS (TAESS) was calculated for both coronary models applying patient-specific physiological data available at the time of imaging and TAESS were categorized into patient-specific tertiles (low, medium, and high). The study concluded that this methodology can accurately assess the TAESS distribution non-invasively from CTA and demonstrated a good correlation with TAESS calculated using IVUS/OCT 3D reconstructed models.[28] Further investigations have been performed to compare computation of plaque and vascular characteristics using intravascular imaging vs. non-invasive assessment. Conte et al,[19] assessed plaque volume quantification by 64-slice vs 256-slice CCTA using IVUS-based measurements as a reference standard, utilizing 118 patients from a large Italian registry. They found a higher correlation for plaque volume quantification by CCTA vs. IVUS which was particularly evident using the more current 256-slice CCTA in comparison with the older 64-slice CCTA. Previous experience in evaluating coronary artery variables by CCTA vs. IVUS has shown that CCTA underestimates lumen cross sectional area compared to IVUS while it overestimates the vessel area.[29]

We observed that there were pathobiologically minor differences in absolute values of local minimal, maximal, and average ESS utilizing CCTA-based vs IVUS-based imaging (well under 1.0 Pa, and as low as 0.23 Pa difference in minimal ESS values). (Table 6). Previous prognostic studies underscore the clinically minor significance of these absolute differences.[2,22]

In our study, we demonstrate good agreement between CCTA-derived ESS computation compared to IVUS-based computation in evaluating both anatomical plaque characteristics (lumen area, plaque area, vessel area) and the most important ESS metrics (Minimal ESS, Maximal ESS, Average ESS) as both continuous and categorical measures.

4.4. 256-slice CCTA vs.64 slice-CCTA

Additive to previously published studies, this present study also included a direct comparison of 64-slice versus 256-slice CCTA to determine the influence of iteratively improving CT hardware technologies on ESS computation. In the present study 256-slice CCTA was comparable to 64-slice CCTA for assessment of anatomical plaque and artery features and statistically similar for assessment of ESS metrics, with absolute differences in Pa between the two modalities demonstrated to be pathobiologically minor. Given the rapidly updating landscape of CCTA hardware technologies—including photon counting detector CT scanners, fast pitch helical scanners and so on—and the differences in CCTA image acquisition protocols (e.g., contrast type and rate of injection, iterative reconstruction, etc.), future studies will be required to determine the diagnostic performance of ESS measures across all of these potentially influential variables.

4.5. Limitations

This study is not without limitations. First, while larger than nearly all prior studies before it, our present study evaluated a relatively small cohort from 256-and 64-slice CT scanners; and future studies should corroborate our findings in different cohorts and on different CT platform technologies. Second, while we enrolled patients within 90 days of CCTA and IVUS, it is possible that temporal differences may have occurred that influence coronary artery volumes, and these may have contributed to differences in ESS measurements between CCTA and IVUS. Third, while we have proven that diagnostic performance of CCTA-based ESS is similar to IVUS-based ESS, our present study lacks patient-centered outcomes and confirmation of its prognostic value. Fourth, CCTA lumen tend to be smaller based on the previous studies which could have an effect on the CFD analysis, but we think that with the new CT technologies (single photon, dual sources CT, flash helical CT) and improvement of image reconstruction, such discrepancies could be reduced. We performed this study as a foundational study to be followed by a large-scale evaluation of ESS in clinical outcomes to demonstrate its validity, and ESS-based prognosis will be evaluated by our group subsequently.

5. Conclusion

Non-invasive computation of ESS by CCTA-based techniques demonstrates similar diagnostic performance to IVUS-based approaches. Evaluation of the clinical import of ESS in patients undergoing CCTA is now indicated.

Supplementary Material

Refer to Web version on PubMed Central for supplementary material.

Source of Funding

We received support from National Institute of Health, grant 1R01 HL146144.

Mona Ahmed received funding from ; The Swedish heart-lung foundation (application no. 20200165), The Swedish research council (application no. 2021-00456)

Peter H Stone reports financial support was provided by the National Institute of Health. Mona Ahmed reports financial support was provided by Swedish Heart and Lung Association. Mona Ahmed reports financial support was provided by Swedish Research Council. Peter H Stone reports financial support was provided by Schaubert Family. Non

Non-standard Abbreviations and Acronyms.

IVUS	Intravascular ultrasound
CCTA	coronary computed tomography angiography
ESS	endothelial shear stress
CFD	computational fluid dynamics
CAD	coronary artery disease
MACE	major adverse cardiac events
OCT	optical coherence tomography
EEM	external elastic membrane
BMI	body mass index

References

1. Samady H, Eshtehardi P, McDaniel MC, Suo J, Dhawan SS, Maynard C, Timmins LH, Quyyumi AA, Giddens DP. Coronary artery wall shear stress is associated with progression and transformation of atherosclerotic plaque and arterial remodeling in patients with coronary artery disease. Circulation. 2011;124:779–788. [PubMed: 21788584]
2. Stone PH, Maehara A, Coskun AU, Maynard CC, Zaromytidou M, Siasos G, Andreou I, Fotiadis D, Stefanou K, Papafaklis M, et al. Role of Low Endothelial Shear Stress and Plaque Characteristics in the Prediction of Nonculprit Major Adverse Cardiac Events: The PROSPECT Study. JACC Cardiovasc Imaging. 2018;11:462–471. [PubMed: 28917684]
3. Yamamoto E, Siasos G, Zaromytidou M, Coskun AU, Xing L, Bryniarski K, Zanchin T, Sugiyama T, Lee H, Stone PH, et al. Low Endothelial Shear Stress Predicts Evolution to High-Risk Coronary

Plaque Phenotype in the Future: A Serial Optical Coherence Tomography and Computational Fluid Dynamics Study. Circ Cardiovasc Interv. 2017;10:e005455.

4. Oemrawsingh RM, Cheng JM, García-García HM, van Geuns R-J, de Boer SPM, Simsek C, Kardys I, Lenzen MJ, van Domburg RT, Regar E, et al. Near-infrared spectroscopy predicts cardiovascular outcome in patients with coronary artery disease. J Am Coll Cardiol. 2014;64:2510–2518. [PubMed: 25500237]
5. Waksman R, Di Mario C, Torguson R, Ali ZA, Singh V, Skinner WH, Artis AK, Cate TT, Powers E, Kim C, et al. Identification of patients and plaques vulnerable to future coronary events with near-infrared spectroscopy intravascular ultrasound imaging: a prospective, cohort study. Lancet. 2019;394:1629–1637. [PubMed: 31570255]
6. Erlinge D, Maehara A, Ben-Yehuda O, Bøtker HE, Maeng M, Kjøller-Hansen L, Engstrøm T, Matsumura M, Crowley A, Dressler O, et al. Identification of vulnerable plaques and patients by intracoronary near-infrared spectroscopy and ultrasound (PROSPECT II): a prospective natural history study. Lancet. 2021;397:985–995. [PubMed: 33714389]
7. Calvert PA, Obaid DR, O'Sullivan M, Shapiro LM, McNab D, Densem CG, Schofield PM, Braganza D, Clarke SC, Ray KK, et al. Association between IVUS findings and adverse outcomes in patients with coronary artery disease: the VIVA (VH-IVUS in Vulnerable Atherosclerosis) Study. JACC Cardiovasc Imaging. 2011;4:894–901. [PubMed: 21835382]
8. Cheng JM, Garcia-Garcia HM, de Boer SPM, Kardys I, Heo JH, Akkerhuis KM, Oemrawsingh RM, van Domburg RT, Ligthart J, Witberg KT, et al. In vivo detection of high-risk coronary plaques by radiofrequency intravascular ultrasound and cardiovascular outcome: results of the ATHEROREMO-IVUS study. Eur Heart J. 2014;35:639–647. [PubMed: 24255128]
9. Stone GW, Maehara A, Lansky AJ, de Bruyne B, Cristea E, Mintz GS, Mehran R, McPherson J, Farhat N, Marso SP, et al. A prospective natural-history study of coronary atherosclerosis. N Engl J Med. 2011;364:226–235. [PubMed: 21247313]
10. Chatzizisis YS, Coskun AU, Jonas M, Edelman ER, Feldman CL, Stone PH. Role of endothelial shear stress in the natural history of coronary atherosclerosis and vascular remodeling: molecular, cellular, and vascular behavior. J Am Coll Cardiol. 2007;49:2379–2393. [PubMed: 17599600]
11. Brown AJ, Teng Z, Evans PC, Gillard JH, Samady H, Bennett MR. Role of biomechanical forces in the natural history of coronary atherosclerosis. Nat Rev Cardiol. 2016;13:210–220. [PubMed: 26822720]
12. Kumar A, Thompson EW, Lefieux A, Molony DS, Davis EL, Chand N, Fournier S, Lee HS, Suh J, Sato K, et al. High Coronary Shear Stress in Patients With Coronary Artery Disease Predicts Myocardial Infarction. J Am Coll Cardiol. 2018;72:1926–1935. [PubMed: 30309470]
13. Thondapu V, Mamon C, Poon EKW, Kurihara O, Kim HO, Russo M, Araki M, Shinohara H, Yamamoto E, Dijkstra J, et al. High spatial endothelial shear stress gradient independently predicts site of acute coronary plaque rupture and erosion. Cardiovasc Res. 2021;117:1974–1985. [PubMed: 32832991]
14. Kishi S, Magalhães TA, Cerci RJ, Matheson MB, Vavere A, Tanami Y, Kitslaar PH, George RT, Brinker J, Miller JM, et al. Total coronary atherosclerotic plaque burden assessment by CT angiography for detecting obstructive coronary artery disease associated with myocardial perfusion abnormalities. J Cardiovasc Comput Tomogr. 2016;10:121–127. [PubMed: 26817414]
15. Lee JM, Choi G, Koo B-K, Hwang D, Park J, Zhang J, Kim K-J, Tong Y, Kim HJ, Grady L, et al. Identification of High-Risk Plaques Destined to Cause Acute Coronary Syndrome Using Coronary Computed Tomographic Angiography and Computational Fluid Dynamics. JACC Cardiovasc Imaging. 2019;12:1032–1043. [PubMed: 29550316]
16. Mortensen MB, Dzaye O, Steffensen FH, Bøtker HE, Jensen JM, Rønnow Sand NP, Kragholm KH, Sørensen HT, Leipsic J, Mæng M, et al. Impact of Plaque Burden Versus Stenosis on Ischemic Events in Patients With Coronary Atherosclerosis. J Am Coll Cardiol. 2020;76:2803–2813. [PubMed: 33303068]
17. Ferraro RA, van Rosendael AR, Lu Y, Andreini D, Al-Mallah MH, Cademartiri F, Chinnaiyan K, Chow BJW, Conte E, Cury RC, et al. Non-obstructive high-risk plaques increase the risk of future culprit lesions comparable to obstructive plaques without high-risk features: the ICONIC study. Eur Heart J Cardiovasc Imaging. 2020;21:973–980. [PubMed: 32535636]

18. Lee S-E, Sung JM, Andreini D, Al-Mallah MH, Budoff MJ, Cademartiri F, Chinnaiyan K, Choi JH, Chun EJ, Conte E, et al. Per-lesion versus per-patient analysis of coronary artery disease in predicting the development of obstructive lesions: the Progression of AtheRosclerotic PlAque DetermIned by Computed TmoGraphic Angiography Imaging (PARADIGM) study. Int J Cardiovasc Imaging. 2020;36:2357–2364. [PubMed: 32779077]

19. Conte E, Mushtaq S, Pontone G, Li Piani L, Ravagnani P, Galli S, Collet C, Sonck J, Di Odoardo L, Guglielmo M, et al. Plaque quantification by coronary computed tomography angiography using intravascular ultrasound as a reference standard: a comparison between standard and last generation computed tomography scanners. Eur Heart J Cardiovasc Imaging. 2020;21:191–201. [PubMed: 31093656]

20. Mintz GS, Nissen SE, Anderson WD, Bailey SR, Erbel R, Fitzgerald PJ, Pinto FJ, Rosenfield K, Siegel RJ, Tuzcu EM, et al. American College of Cardiology Clinical Expert Consensus Document on Standards for Acquisition, Measurement and Reporting of Intravascular Ultrasound Studies (IVUS). A report of the American College of Cardiology Task Force on Clinical Expert Consensus Documents. J Am Coll Cardiol. 2001;37:1478–1492. [PubMed: 11300468]

21. Tomaniak M, Katagiri Y, Modolo R, de Silva R, Khamis RY, Bourantas CV, Torii R, Wentzel JJ, Gijsen FJH, van Soest G, et al. Vulnerable plaques and patients: state-of-the-art. Eur Heart J. 2020;41:2997–3004. [PubMed: 32402086]

22. Stone PH, Saito S, Takahashi S, Makita Y, Nakamura S, Kawasaki T, Takahashi A, Katsuki T, Nakamura S, Namiki A, et al. ; PREDICTION Investigators. Prediction of progression of coronary artery disease and clinical outcomes using vascular profiling of endothelial shear stress and arterial plaque characteristics: the PREDICTION Study. Circulation. 2012 Jul 10;126(2):172–81. [PubMed: 22723305]

23. Hetterich H, Jaber A, Gehring M, Curta A, Bamberg F, Filipovic N, Rieber J. Coronary computed tomography angiography based assessment of endothelial shear stress and its association with atherosclerotic plaque distribution in-vivo. PLoS One. 2015;10:e0115408.

24. Rybicki FJ, Melchionna S, Mitsouras D, Coskun AU, Whitmore AG, Steigner M, Nallamshetty L, Welt FG, Bernaschi M, Borkin M, et al. Prediction of coronary artery plaque progression and potential rupture from 320-detector row prospectively ECG-gated single heart beat CT angiography: Lattice Boltzmann evaluation of endothelial shear stress. Int J Cardiovasc Imaging. 2009;25:289–299. [PubMed: 19043805]

25. Park J-B, Choi G, Chun EJ, Kim HJ, Park J, Jung J-H, Lee M-H, Otake H, Doh J-H, Nam C-W, et al. Computational fluid dynamic measures of wall shear stress are related to coronary lesion characteristics. Heart. 2016;102:1655–1661. [PubMed: 27302987]

26. Adriaenssens T, Allard-Ratick MP, Thondapu V, Sugiyama T, Raffel OC, Barlis P, Poon EKW, Araki M, Nakajima A, Minami Y, et al. Optical Coherence Tomography of Coronary Plaque Progression and Destabilization: JACC Focus Seminar Part 3/3. J Am Coll Cardiol. 2021;78:1275–1287. [PubMed: 34531029]

27. Bulant CA, Blanco PJ, Maso Talou GD, Bezerra CG, Lemos PA, Feijóo RA. A head-to-head comparison between CT- and IVUS-derived coronary blood flow models. J Biomech. 2017;51:65–76. [PubMed: 27939753]

28. Eslami P, Hartman EMJ, Albaghadai M, Karady J, Jin Z, Thondapu V, Cefalo NV, Lu MT, Coskun A, Stone PH, et al. Validation of Wall Shear Stress Assessment in Non-invasive Coronary CTA versus Invasive Imaging: A Patient-Specific Computational Study. Ann Biomed Eng. 2021;49:1151–1168. [PubMed: 33067688]

29. Doh J-H, Koo B-K, Nam C-W, Kim J-H, Min JK, Nakazato R, Silalahi T, Prawira H, Choi H, Lee SY, et al. Diagnostic value of coronary CT angiography in comparison with invasive coronary angiography and intravascular ultrasound in patients with intermediate coronary artery stenosis: results from the prospective multicentre FIGURE-OUT (Functional Imaging criteria for GUiding REview of invasive coronary angiOgraphy, intravascular Ultrasound, and coronary computed Tomographic angiography) study. Eur Heart J Cardiovasc Imaging. 2014;15:870–877. [PubMed: 24513881]

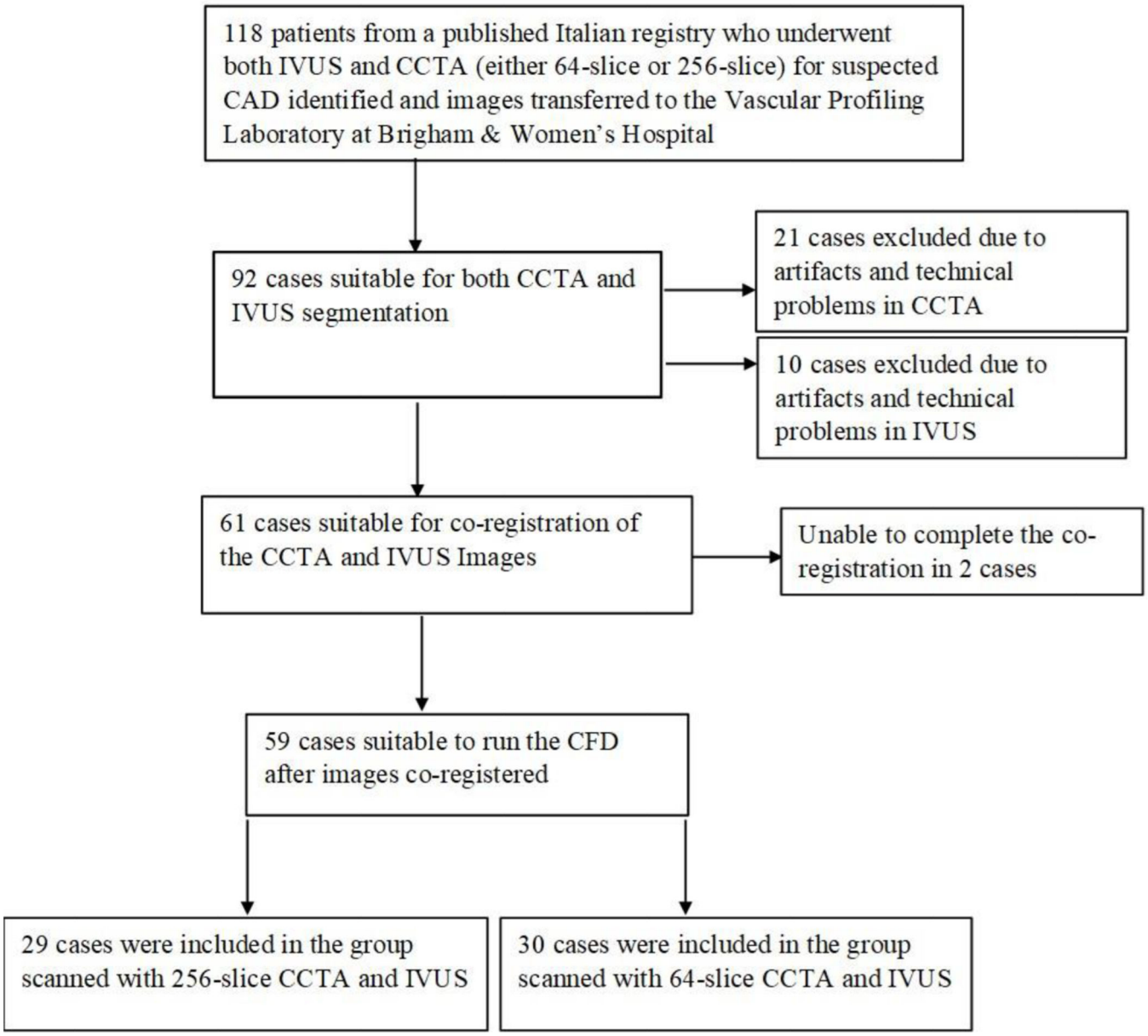

Figure 1:
Study Flow Chart

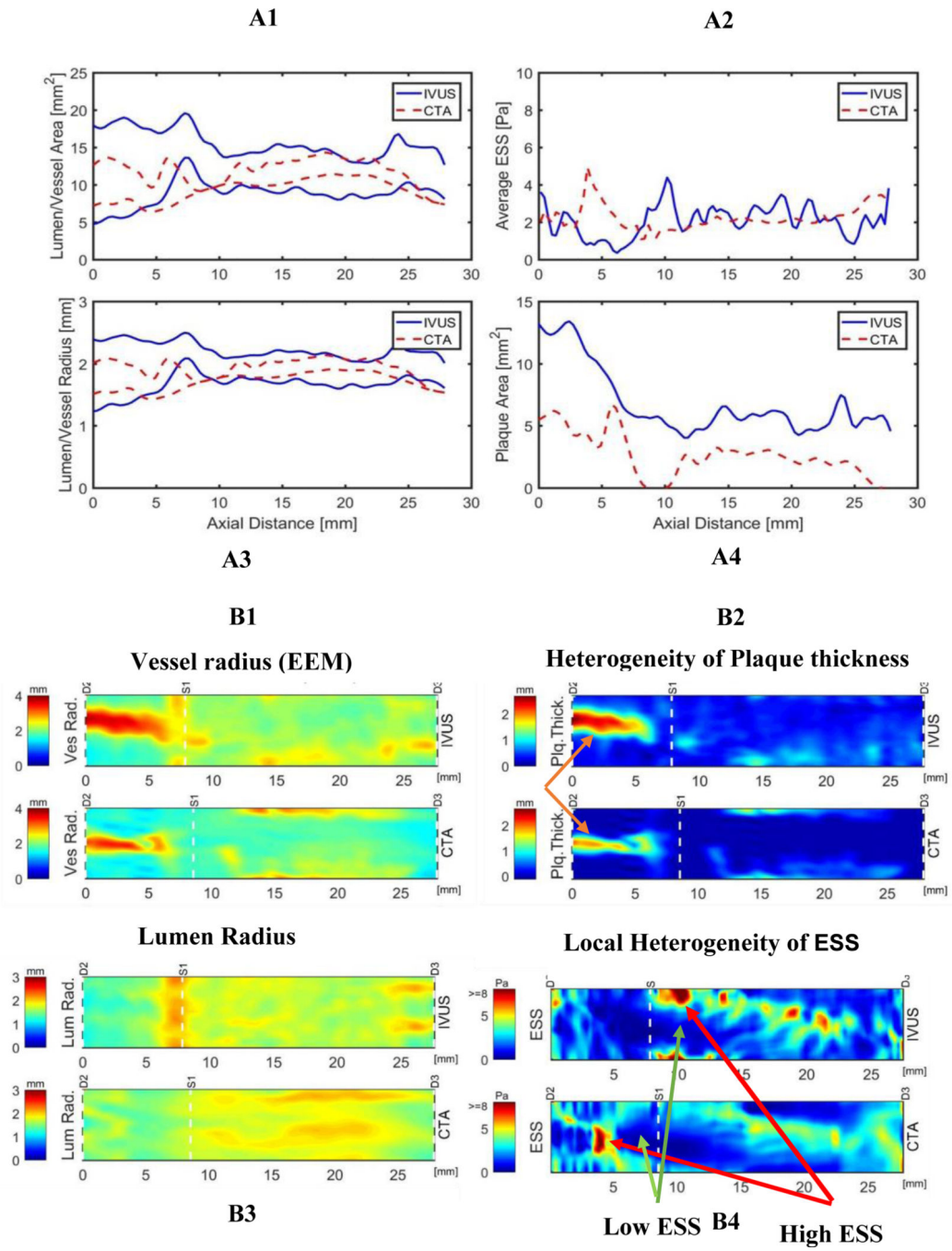

Figure 2: A1-A4: comparison of vascular features and ESS metrics by CCTA vs. IVUS. B1-B4: images 3D reconstruction and color-coded topographical map of the same patient.

CCTA= coronary computed tomography angiography, EEM = external elastic membrane, IVUS=intravascular ultrasound, ESS=endothelial shear stress, Plq Thick = plaque thickness

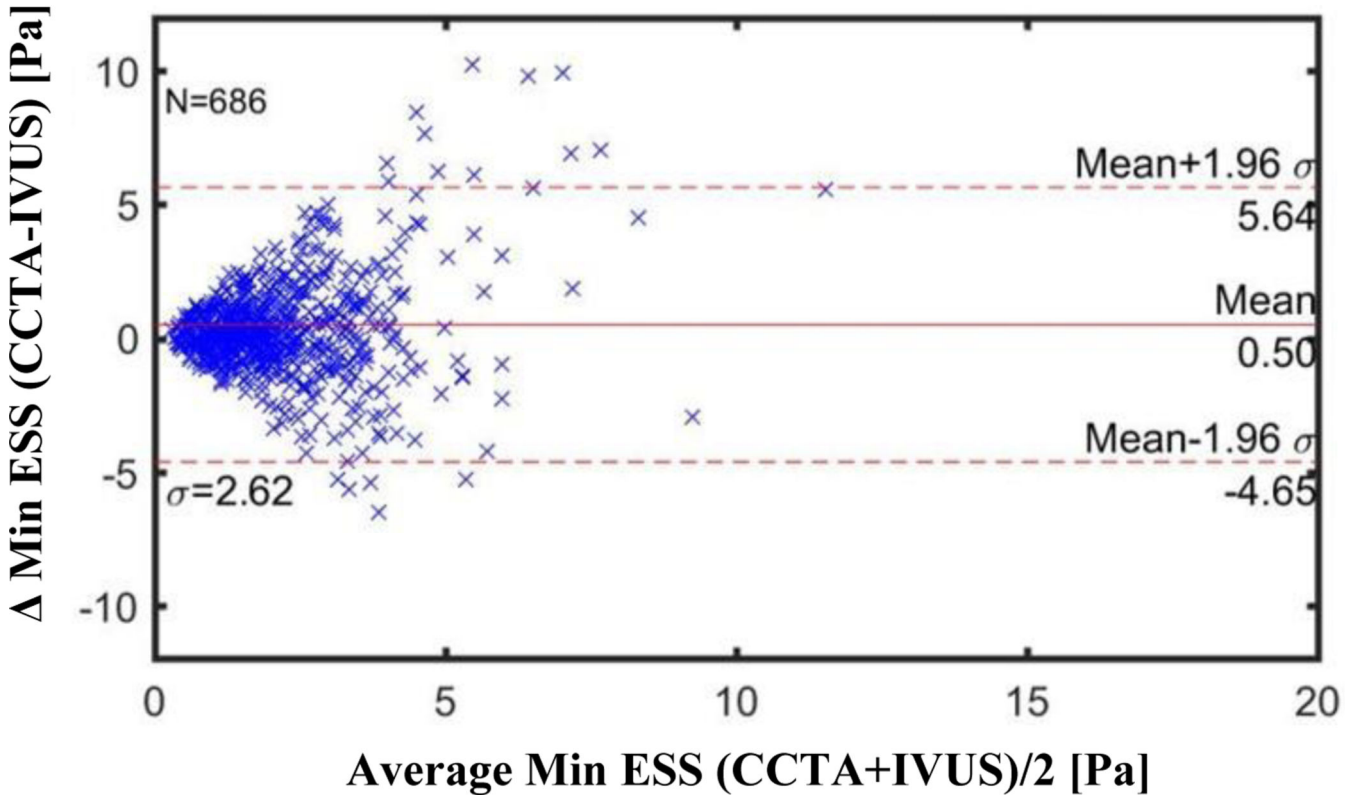

Figure 3: Bland-Altman Plots of Minimal ESS by CCTA vs by IVUS for All CCTA Methods (Combined 256-slice and 64-slice methods)

CCTA= coronary computed tomography angiography

IVUS=intravascular ultrasound

Each marker (N=686) corresponds to average value over 0.3 mm thick sub segment

Mean difference: Combined 256+64 slice CCTA: −0.50 Pa (CI −0.696 to −0.303)

256-slice CCTA: −0.23 Pa (CI −0.440 to −0.028)

64-slice CCTA: −0.75 Pa (CI −1.080 to −0.422)

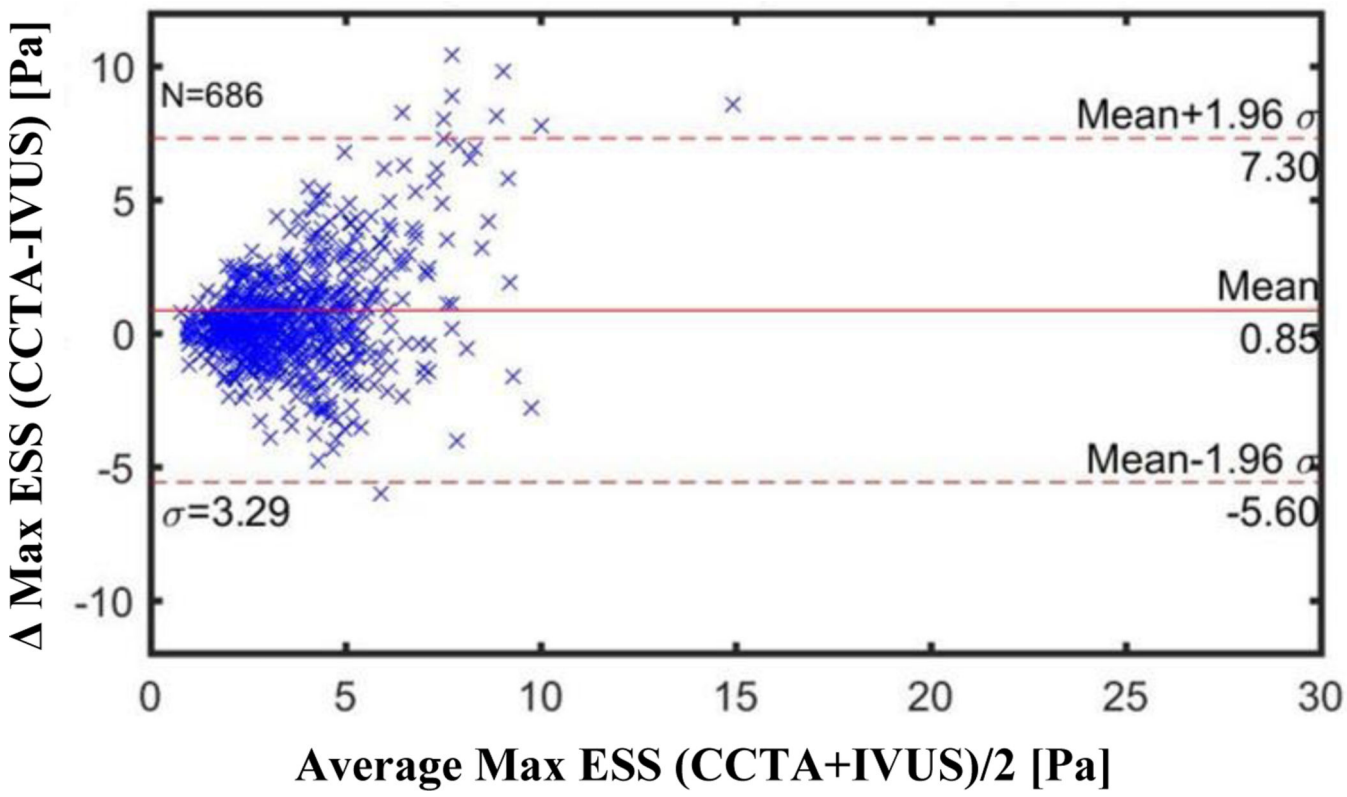

Figure 4: Bland-Altman Plots of Maximal ESS by CCTA vs by IVUS for All CCTA Methods (Combined 256-slice method and 64-slice methods)

CCTA= coronary computed tomography angiography

IVUS=intravascular ultrasound

Each marker (N=686) corresponds to average value over ~0.3 mm thick sub segment

Mean difference: Combined 256+64-slice CCTA: −0.85 Pa (CI −1.094 to −0.601)

256-slice CCTA: −0.52 Pa (CI −0.759 to −0.288)

64-slice CCTA: −1.15 Pa (CI −1.579 to −0.731)

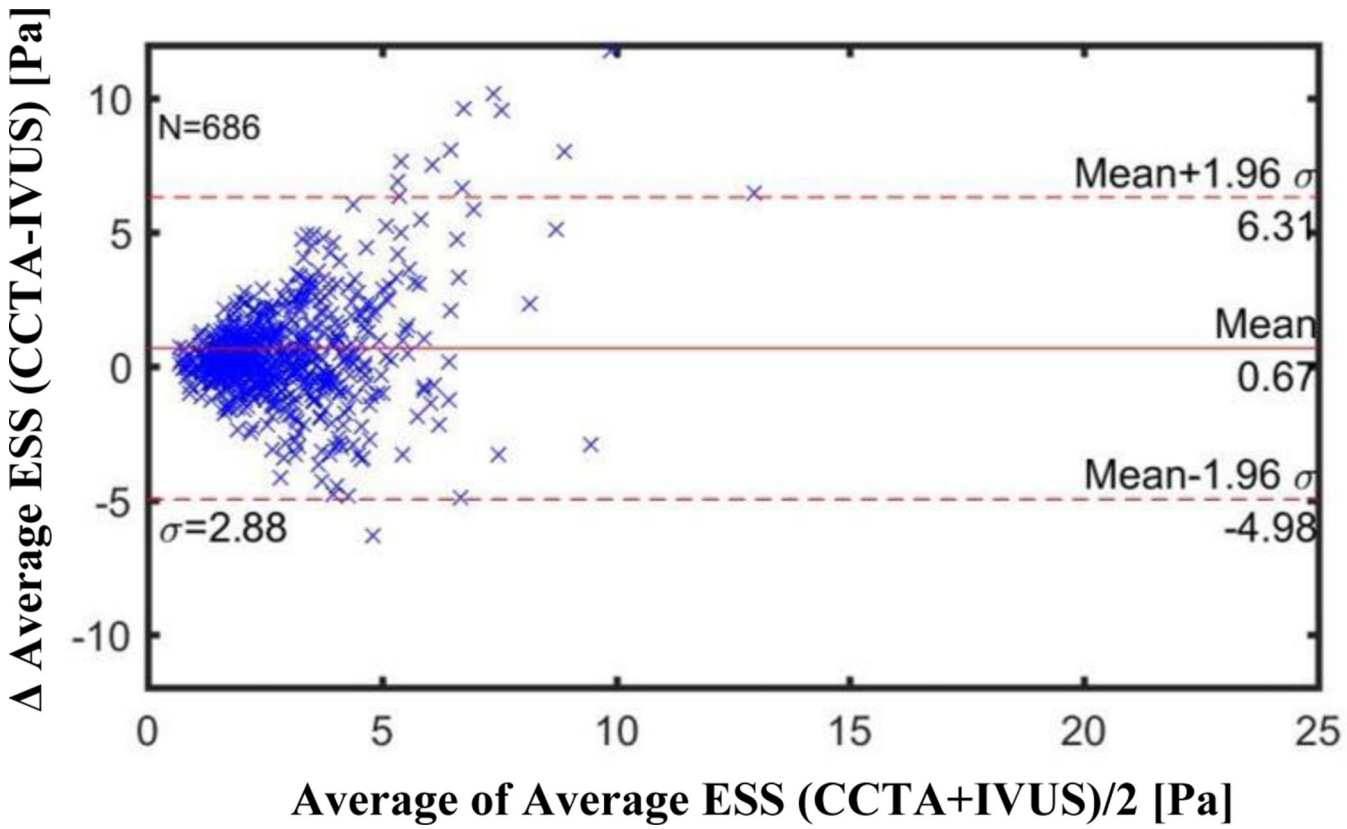

Figure 5: Bland-Altman Plots of Average ESS by CCTA vs by IVUS for All CCTA methods (Combined 256- slice method and 64-slice method)

CCTA=coronary computed tomography angiography, IVUS=intravsacular ultrasound

Each marker (N=686) corresponds to average value over ~0.3 mm thick sub segment

Mean difference: Combined 256+64 slice CCTA: −0.67 Pa (CI −0.885 to −0.453)

256-slice CCTA: −0.37 Pa (CI −0.586 to −0.158)

64-slice CCTA: −0.95 Pa (CI −1.317 to −0.583)

Table 1:

Demographic and Clinical Characteristics of Patient Cohort

	All Patients (n=59)	64-slice CT (n=30)	256-slice CT (n=29)	P value
Age, years (mean ± SD)	67 ± 9	67 ± 10	67 ± 9	1.0
Sex (M), n (%)	47 (79.6)	24 (80)	23 (79.3)	0.81
BMI, kg/m2 (mean ± SD)	25 ± 2	24.9 ± 2.1	25.1 ± 3	0.69
Hypertension, n (%)	31(52.5)	18 (60)	14 (48.2)	0.19
Current smoker, n (%)	16 (27.1)	11 (36)	6 (20.9)	0.10
Hyperlipidemia, n (%)	26 (44)	12 (40)	14 (48.2)	0.57
Diabetes, n (%)	10 (16.9)	5 (16.6)	5 (17.2)	0.80
Family history of CAD, n (%)	16 (27.1)	8 (26.6)	8 (27.5)	0.83

Values are presented as mean± SD for continuous variables and n (%) for categorical variables. n= number of patients. BMI=body mass index, CAD=coronary artery disease, CT=computed tomography

Table 2.

Comparison of IVUS vs All CCTAs (Combined 64-slice and 256-slice): Anatomical plaque characteristics and ESS measurements

Metric	IVUS (n=686)	CCTA (n=686)	Correlation Coefficient	P value*
Vessel Area (mm^2)	12.7 ± 4.3	10.7 ± 4.5	0.63	<0.0001
Lumen Area (mm^2)	6.8 ± 2.7	5.6 ± 2.7	0.43	<0.002
Plaque Area (mm^2)	5.9 ± 2.9	5.1 ± 3.2	0.52	<0.0001
MLA per artery (mm^2)	4.5 ± 1.3	4.1 ± 1.5	0.67	<0.0001
Average ESS (Pa)	2.6 ± 1.5	3.3 ± 3.0	0.35	<0.042
Plaque 90° arc Min ESS (Pa)	2.0 ± 1.4	2.5 ± 2.6	0.28	<0.55
Plaque 90° arc Max ESS (Pa)	3.3 ± 1.6	4.2 ± 3.6	0.42	<0.0004

Values are presented as mean± SD for continuous variables, n= number of analyzed segments, CCTA= coronary computed tomography angiography, MLA=minimal luminal area, Min ESS= minimal endothelial shear stress, Max ESS= maximal endothelial shear stress, Average ESS=average endothelial shear stress

P value

* = P value of the correlation coefficient, correlation coefficient is different from r=0.25

Table 3.

Comparison of IVUS vs CCTA:Separately 64-slice vs 256-slice (continuous variables)

Metric	IVUS (n=686)	CCTA (n=686)	Correlation Coefficient (P-value*)	P value of the correlation coefficient 64-slice vs. 256 slices**
Vessel area (mm^2)				
256-slice CCTA (n=334)	13.1±4.2	11.1±4.5	0.60 (p<0.0001)	P=0.40
64-slice CCTA (n=352)	12.4±4.5	10.3±4.5	0.64 (p<0.0001)	
Lumen area (mm^2)				
256-slice CCTA (n=334)	6.8±2.7	5.6±2.7	0.41 (p<0.0001)	P=0.52
64-slice CCTA (n=352)	6.7±2.8	5.0±2.4	0.45 (p=0.002)	
Plaque area (mm^2)				
256-slice CCTA (n=334)	6.1±2.9	4.9± 3.1	0.67 (p<0.0001)	P=0.81
64-slice CCTA (n=352)	5.8±2.9	5.3±3.3	0.68 (p<0.0001)	
MLA per artery (mm^2)				
256-slice CCTA (n=334)	5.0±2.0	4.1±1.3	0.61(p<0.0001)	P=0.0004
64-slice CCTA (n=352)	4.0±1.2	3.0±1.4	0.41(p=0.24)	
Average ESS (Pa)				
256-slice CCTA (n=334)	2.6±1.4	2.9 ±2.1	0.41 (p<0.0001)	P=0.23
64-slice CCTA (n=352)	2.7±1.7	3.3±3.7	0.33 (p=0.017)	
Plaque 90° arc MIN ESS (Pa)				
256- slice CCTA (n=334)	1.9± 1.4	2.1±1.8	0.32 (p<0.0001)	P=0.48
64-slice CCTA (n=352)	2.0±1.5	2.8±3.2	0.27 (p<0.008)	
Plaque 90° arc MAX ESS (Pa)				
256-slice CCTA (n=334	3.3 ±1.6	3.8±2.5	0.49 (p<0.0001)	P=0.19
64-slice CCTA (n=352)	3.4 ±1.7	4.6±4.4	0.41 (p=0.007)	

Values are presented as mean± SD for continuous variables, n= number of analyzed segments, CCTA= coronary computed tomography angiography, IVUS=intravascular ultrasound, Min ESS= minimal endothelial shear stress, Max ESS= maximal endothelial shear stress, Average ESS=average endothelial shear stress

*Correlation coefficient is different from r=0.25

**Comparison of 2 correlation coefficients

Table 4:

Comparison of IVUS vs CCTA in ESS Environment: All CCTA; 256-slice vs 64-slice (categorical variables)

Metric	IVUS (n=686))	CCTA (n=686))
3-mm segment with min ESS < 1.0 Pa	**Low ESS**	
All CCTA (n=686)	174 (25.4%)	134 (19.5%)
256-slice CCTA (n=334)	85 (25.4%)	65 (19.5%)
64-slice CCTA (n=352)	89 (25.3%)	69 (19.6%)
3-mm segment with avg ESS 1.0 – 2.5 Pa	**Physiologic ESS**	
All CCTA (n=686)	349 (50.9%)	307 (44.8%)
256-slice CCTA (n=334)	187 (56.0%)	163 (44.8%)
64-slice CCTA (n=352)	162 (46.0%)	144 (40.9%)
3-mm segment with avg ESS 2.5 – 5.0 Pa	**High ESS**	
All CCTA (n=686)	246 (35.9%)	262 (38.2%)
256-slice CCTA (n=334)	106 (31.7%)	133 (39.8%)
64-slice CCTA (n=352)	140 (39.8%)	129 (36.6%)
3-mm segment with avg ESS 5.0 – 7.0 Pa	**Higher ESS**	
All CCTA (n=686)	39 (5.7%)	56 (8.2%)
256-slice CCTA (n=334)	16 (4.8%)	21 (6.3%)
64-slice CCTA (n=352)	23 (6.5%)	35 (9.9%)
3-mm segment with max ESS >7 Pa	**Very High ESS**	
All CCTA (n=686)	19 (2.8%)	68 (9.9%)
256-slice CCTA (n=334)	9 (2.7%)	18 (5.4%)
64-slice CCTA (n=352)	10 (2.8%)	50 (14.2%)

Values are presented as n (%) for categorical variables, n= number of analyzed segments CCTA= coronary computed tomography angiography, IVUS=intravascular ultrasound, Min ESS= minimal endothelial shear stress measured over a continuous 90° arc segment on each 3-mm subsegment, Max ESS= maximal endothelial shear stress, Avg ESS=average endothelial shear stress measured over a continuous 90° arc segment on each 3-mm subsegment. Some samples may be part of more than 1 category. For example, a sample that may have a physiological average ESS value, can have a Min ESS value lower than physiological or max ESS value higher than physiological, and therefore can be counted in Physiological ESS, low min ESS and/or high max ESS categories.

Agreement for all CCTA, kappa=0.25, p<0.0001

Agreement for 256 slice, kappa=0.26, p<0.0001

Agreement for 64 slice, kappa=0.24, p<0.0001

Table 5.

Comparison of Categories of ESS by Per-segment Analysis Coronary CT Angiography vs Intravascular Ultrasound

(A)

IVUS Category of Avg ESS	CCTA Category for Average ESS: Low	Physio	High	Higher	Very H	
Low	8	22	11	2	0	43
Physio	13	209	96	19	12	349
High	5	67	135	24	15	246
Higher	0	8	18	8	5	39
Very H	0	1	2	3	3	9
Total	26	307	262	56	35	686

IVUS Category of Avg ESS	CCTA Category for Average ESS: Low	Physio	High	Higher	Very H	
Low	18.6%	51.2%	25.6%	4.7%	0.0%	100%
Physio	3.7%	59.9%	27.5%	5.4%	3.4%	100%
High	2.0%	27.2%	54.9%	9.8%	6.1%	100%
Higher	0.0%	20.5%	46.2%	20.5%	12.8%	100%
Very H	0.0%	11.1%	22.2%	33.3%	33.3%	100%

(B)

IVUS Category of Min ESS	CCTA Category for Min ESS: Low	Physio	High	Higher	Very H	
Low	**58**	81	23	6	6	174
Physio	58	**190**	69	9	8	334
High	14	49	**70**	8	6	147
Higher	3	9	9	**1**	2	24
Very H	1	0	3	0	**3**	7
Total	134	329	174	24	25	686

IVUS Category of Min ESS	CCTA Category for Min ESS: Low	Physio	High	Higher	Very H	
Low	33.3%	46.6%	13.2%	3.4%	3.4%	100%
Physio	17.4%	56.9%	20.7%	2.7%	2.4%	100%
High	9.5%	33.3%	47.6%	5.4%	4.1%	100%
Higher	12.5%	37.5%	37.5%	4.2%	8.3%	100%
Very H	14.3%	0.0%	42.9%	0.0%	42.9%	100%

(C)

IVUS Category of Max ESS	CCTA Category for Max ESS: Low	Physio	High	Higher	Very H	
Low	**0**	11	2	0	0	13
Physio	10	**116**	89	13	3	231
High	2	57	**187**	55	39	340
Higher	0	6	39	**21**	17	83
Very H	0	0	3	7	**9**	19
Total	12	190	320	96	68	686

IVUS Category of Max ESS	CCTA Category for Max ESS: Low	Physio	High	Higher	Very H	
Low	0.0%	84.6%	15.4%	0.0%	0.0%	100%
Physio	4.3%	50.2%	38.5%	5.6%	1.3%	100%
High	0.6%	16.8%	55.0%	16.2%	11.5%	100%
Higher	0.0%	7.2%	47.0%	25.3%	20.5%	100%
Very H	0.0%	0.0%	15.8%	36.8%	47.4%	100%

Values are presented as n and (%) for categorical variables. n= number of analyzed segments, CCTA= coronary computed tomography angiography, IVUS=intravascular ultrasound, Min ESS= minimal endothelial shear stress, Max ESS= maximal endothelial shear stress, Avg ESS=average endothelial shear stress. L=low shear stress i.e. <1.0 Pa, Physio= physiologic shear stress i.e. 1.0 –2.5 Pa, High=high endothelial shear stress i.e. 2.5–5.0 Pa, Higher=higher endothelial shear stress i.e. 5.0 –7.0 Pa, Very H= very high endothelial shear stress i.e. >7 Pa.

Agreement for average ESS, kappa=0.25, p<0.0001, Agreement for min ESS, kappa=0.20, p<0.0001, Agreement for max ESS, kappa=0.22, p<0.0001,

Table 6:

Absolute differences in ESS metrics as measured by IVUS versus the different CCTA imaging methods.

CCTA Method	Mean Difference (Pa)	p- value
Average ESS		
All CCTA	−0.66 Pa	<0.0001
256-Slice	−0.37 Pa	0.006
64-Slice	−0.95 Pa	0.002
Minimal ESS		
All CCTA	−0.49 Pa	<0.0001
256-Slice	−0.23 Pa	0.032
64-Slice	−0.75 Pa	0.004
Maximal ESS		
All CCTA	−0.84 Pa	<0.0001
256-Slice	−0.52 Pa	<0.0001
64-Slice	−1.1 Pa	0.001

CCTA= coronary computed tomography angiography, Avg ESS=average endothelial shear stress, Min ESS= minimal endothelial shear stress, Max ESS= maximal endothelial shear stress,